Tomographic-PIV investigation of the 3D Separation behaviour of a micro-ramp controlled SWBLI

Nayak, Kapileswar; Giepman, Rogier; Schrijer, Ferdinand; van Oudheusden, Bas

Publication date
2017

Document Version
Final published version

Published in
52nd 3AF International Conference on Applied Aerodynamics

Citation (APA)
Nayak, K., Giepman, R., Schrijer, F., & van Oudheusden, B. (2017). Tomographic-PIV investigation of the 3D Separation behaviour of a micro-ramp controlled SWBLI. In *52nd 3AF International Conference on Applied Aerodynamics: 27 – 29 March 2017, Lyon – France* Article FP45-AERO2017-schrijer

52nd 3AF International Conference on Applied Aerodynamics
27 – 29 March 2017, Lyon - France

FP45-AERO2017-schrijer

TOMOGRAPHIC-PIV INVESTIGATION OF THE 3D SEPARATION BEHAVIOUR OF A MICRO-RAMP CONTROLLED SWBLI.

S. Nayak K[(1)], R.H.M. Giepman[(2)], F.F.J. Schrijer[(3)], B.W. van Oudheusden[(4)]

(1) TU Delft Faculty of Aerospace Engineering, Kluyverweg 1, 2629HS Delft, The Netherlands
nykshruthi@gmail.com
(2) TU Delft Faculty of Aerospace Engineering, Kluyverweg 1, 2629HS Delft, The Netherlands
R.H.M.Giepman@tudelft.nl
(3) TU Delft Faculty of Aerospace Engineering, Kluyverweg 1, 2629HS Delft, The Netherlands
F.F.J.Schrijer@tudelft.nl
(4) TU Delft Faculty of Aerospace Engineering, Kluyverweg 1, 2629HS Delft, The Netherlands
B.W.vanOudheusden@tudelft.nl

ABSTRACT

Micro-ramp vortex generators (or micro-ramps) have gained popularity as promising alternatives to boundary layer bleed for high speed flow-control applications. Micro-ramps generate a counter-rotating vortex pair which leads to a more separation resistant boundary layer. Furthermore, they modulate the size of the shock induced separation bubble along the span such that individual cells of three-dimensional separation are formed.

In the current study, the highly three-dimensional nature of such a micro-ramp controlled SWBLI is visualized by using tomographic-PIV. The 3D mean flow field of the interaction is presented, while the 3D separation behaviour is further characterized by the separation probability of the interaction P_{sep} at different wall-parallel planes. The largest reduction in P_{sep} occurs along the micro-ramp centreline where separation is basically eliminated. Additionally, it is found that the total volume of separation is decreased by 70% when compared to an uncontrolled SWBLI.

1. INTRODUCTION

Shock-wave boundary layer interactions (SWBLIs) are complex phenomena that occur frequently in high speed flight. SWBLIs can have catastrophic consequences for the aircraft engine intakes due to shock induced separation and unsteadiness of the interaction. A conventional method of mitigating the negative effects associated to SWBLIs is by employing boundary layer bleed [1] whereby the low momentum part of the boundary layer is removed, making it more resistive to an adverse pressure gradient. Importantly, the mass flow that is removed is not typically re-injected and thus the net engine mass flow rate is reduced. This necessitates an increase in the frontal area of the engine, increasing the weight and drag of the aircraft [2]. Therefore, passive flow control devices such as micro-ramp vortex generators are promising alternatives to boundary layer bleed.

Micro-ramp vortex generators (or micro-ramps) are small wedge like ramp devices that are based on the same principle as conventional vortex generators. Their control authority comes from a pair of counter-rotating vortices which entrains higher momentum fluid from the outer parts of the boundary layer/free stream and transport the higher momentum fluid to the near wall regions [3]. This results in a fuller boundary layer velocity profile which is more separation resistant [3]. Previous studies [3, 4] have shown that due to the action of the micro-ramp, the shock induced separation bubble along the centreline is completely eliminated. When moving away from the micro-ramp centreline, the effectiveness of the micro-ramp reduces and separated flow regions are again observed [4]. Blinde *et al* [5] performed stereoscopic-Particle Image Velocimetry (PIV) studies of micro-ramp arrays, and found that the largest reductions in shock-induced separation occur at outboard locations away from micro-ramp centreline

which is contrary to the results reported by Babinsky *et al* [3] and Giepman *et al* [4].

Hence, given the highly three-dimensional nature of a micro-ramp controlled SWBLI, it is needed to capture the 3D flow organization in the interaction region in order to properly assess the effectiveness of the micro-ramp. Further, Lee *et al* [6] used Large Eddy Simulations (LES) to study the 3D features of the present problem. They found that smaller micro-ramps are more effective than larger micro-ramps in reducing shock-induced separation contrary to the experimental results of [3, 4].

In the present work an experimental approach is taken and fully 3D measurements are performed using tomographic-PIV [7] which has been proven to yield high quality data for supersonic flows [8, 9, 10]. In this investigation, the mean 3D flow fields in the micro-ramp controlled interaction region are characterized. The separation behaviour is further investigated by calculating the separation (i.e. reverse-flow) probability P_{sep} [4] in the entire measurement volume. The reduction in the total volume of separated flow in the interaction region with respect to the uncontrolled interaction is determined as an indicator of the separation control authority.

2. EXPERIMENTAL SETUP

Experiments were performed in the ST-15 blowdown wind tunnel at the Faculty of Aerospace Engineering, Delft University of Technology. The free stream Mach number was equal to 2.0 with a total pressure $p_0 = 3.2 \times 10^5$ Pa and a total temperature $T_0 = 278$ K. This resulted in a unit Reynolds number of 43.5×10^6 m^{-1}. The turbulent boundary layer on the lower wall of the test section was used for the interaction. It had a thickness of $\delta_{99} = 5.2$ mm, while the incompressible displacement and momentum thickness were determined to be $\delta_i^* = 0.67$ mm and $\theta_i^* = 0.51$ mm, respectively, yielding $Re_\theta = 22 \times 10^3$. Furthermore, the incompressible shape factor $H_i = 1.3$. The incident shock wave is generated by a nearly full span 12° shock generator. The inviscid shock impingement location is taken as the origin of the co-ordinate system. The geometry of the micro-ramps used for the controlled interaction is based on the recommendations of Anderson *et al* [11]. A single micro-ramp with a height of 3 mm ($0.58\delta_{99}$) is positioned at 90 mm ($17.3\delta_{99}$) upstream of the inviscid shock impingement location along the centerline of the tunnel. The undisturbed boundary layer parameters are detailed in Tab 1.

The tomographic imaging system consisted of 6 LaVision Imager LX2 cameras placed on either side of the test section as shown in Fig 1. The measurement volume imaged was $6.2\delta \times 2.2\delta \times 4.6\delta$ in the streamwise, wall-normal and spanwise directions respectively. In this measurement region, it was possible to capture only a part of the separation bubble. The cameras had a sensor of 1624 × 1236 pixels with a pixel size of 4.4 µm and were equipped with 75 mm objective lens with f-number $f_\# = 11$. The cameras were equipped with Scheimpflug adapters to align the focal plane in the mid-section of the measurement volume and to maintain the entire measurement volume in focus.

Table 1. Undisturbed boundary layer conditions

Parameter	Value
M_∞	2
p_0	3.2×10^5 N/m^2
T_0	278K
unit Re	43.5×10^6 m^{-1}
Re_θ	22×10^3
δ or δ_{99}	5.2mm
δ_i^*	0.67mm
θ_i^*	0.51mm
H_i	1.3

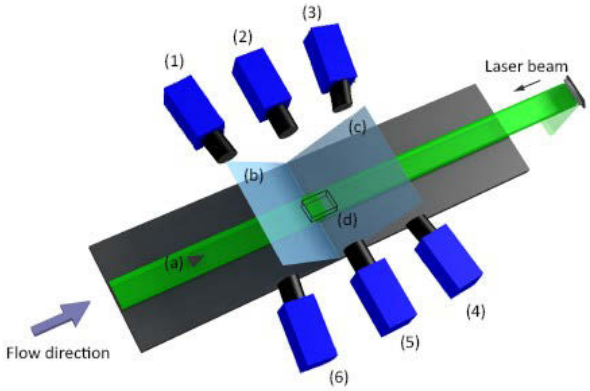

Figure 1. Schematic of the tomographic-PIV set up: cameras (1 – 6), micro-ramp (a), inviscid incident shock wave (b), and reflected shock wave (c), location of the measurement volume (d).

The seeding was provided by a PIVTEC Aerosol generator PivPart45. The Di-ethyl hexyl sebacat (DEHS) tracer particles were distributed into the tunnel by a custom seeding rake. The illumination was provided by a Spectral Physics Quanta Ray double-pulsed Nd-YAG laser (532 nm, 400 mJ per pulse and 6 ns pulse duration) from the back of the tunnel to avoid reflections from the walls. The laser pulse separation time was 0.8 µs and the spatial resolution was 36.1 pixels/mm.

The synchronization of camera trigger signals and laser, as well as the image acquisition were achieved by a LaVision programmable timing unit (PTU) and the DaVis 8.2 software package. The acquired images were pre-processed using DaVis 8.1.6 before the volume-self calibration which proved to be an essential step in the data processing procedure. The average minimum intensity was subtracted from all images to reduce the background noise. This was followed by the 'subtract sliding minimum' filter using a kernel of 31 pixels.

Uniform particle image intensity was obtained between different images by normalization of particle intensity on a larger scale using the 'normalize using local average' filter. Finally, a constant 40 counts was subtracted from every pixel to remove the remaining background noise.

Table 2. Tomographic PIV recording parameters

Parameter	Value
Digital Image resolution	36.1 pixels/mm
Measurement volume	6.2δ×2.2δ×4.6δ
Objective focal length	75mm
f-number $f_{\#}$	11
Laser pulse separation time	0.8μs
Final interrogation volume	48×48×48 voxels or 1.3×1.3×1.3 mm^3

The images so obtained were used for the volume self-calibration procedure. Following this, a Gaussian smoothing filter with a 3×3 kernel was applied and each pixel was multiplied by a constant factor of 10 to further improve the particle images for volume reconstruction and correlation. The fastMART option was used for the volume reconstruction procedure. The reconstructed volumes were correlated using the 'Direct correlation' option and the interrogation window size was gradually reduced from 128×128×128 voxels to the final interrogation window size of 48×48×48 voxels. All the tomographic-PIV parameters are summarized in Tab 2.

3. VOLUMETRIC VISUALIZATION

The volumetric representations of the mean flow organization in the uncontrolled and micro-ramp controlled interactions are presented in Fig 2. Due to laser light reflections from the wall, the first reliable measurement point is located at $y/\delta = 0.3$. Because of this, reversed flow regions are not observed in the mean flow results. In addition, the limited spatial resolution of the PIV measurements (approximately equal to a window size) results in the modulation of small reversed flow regions. Therefore, the outline of the separated region is rendered by an iso-surface for $U = 0.1U_\infty$ shown in purple. The green contour represents $U = 0.75U_\infty$ iso-surface approximately indicating compression and expansion regions. In the uncontrolled interaction in Fig. 2a, this high-velocity iso-surface shows a high degree of spanwise homogeneity indicating that the reflected shock is rather planar. However, the counter-rotating vortices generated by the micro-ramp greatly alter the pre-dominant two-dimensionality of the high velocity iso-surface, as can be seen in Fig. 2b. The primary counter-rotating vortices are visualized using the streamwise vorticity ω_x and are shown in red and blue. The counter-rotating vortices have similar magnitude but opposite directions of rotation.

Fig. 3 shows the mean streamwise velocity contours for the uncontrolled and controlled interactions on a wall parallel plane at $y/\delta = 0.3$. The incoming boundary layer is fuller due to the action of the micro-ramp. Hence, the boundary layer deceleration due to the shock is postponed downstream. The predominant two-dimensionality of the interaction is distorted by the introduction of the micro-ramps, as seen in Fig. 3b, and the separation bubble (as represented by the region where $U/U_\infty<0.1$) is completely eliminated along the micro-ramp centreline. However, at outboard locations the size of the separation bubble remains comparable to its size in the uncontrolled interaction. Further at $y/\delta = 0.5$, a small pocket enclosing the $U < 0.1U_\infty$ of ~4 mm^2 is observed in the controlled interaction in Fig. 4(b). This indicates a redistribution of separated flow due to the counter-rotating action of the primary vortices.

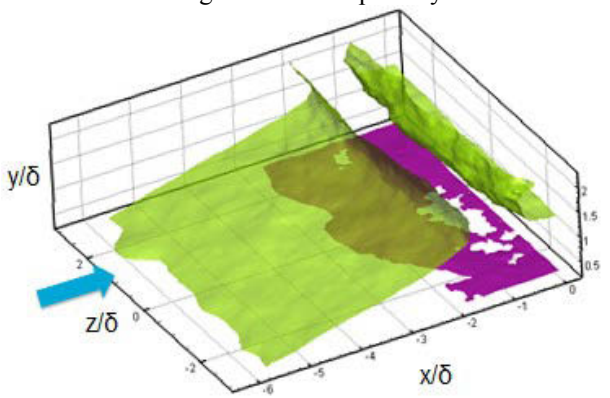

(a) Uncontrolled interaction

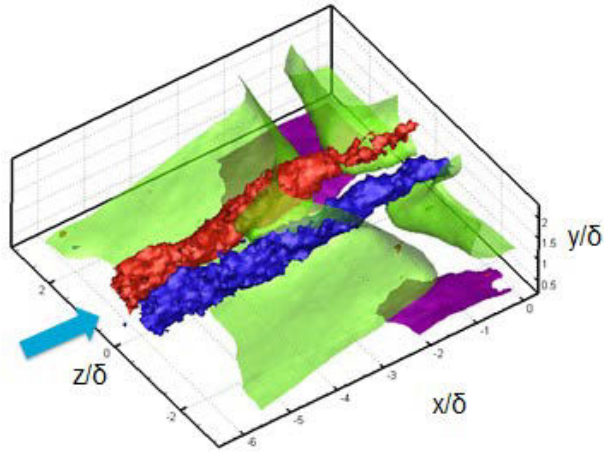

(b) Micro-ramp controlled interaction

Figure 2. Volumetric representation of the interaction region. Green iso-surfaces indicate $U = 0.75U_\infty$, purple iso-surfaces indicate $U = 0.1\ U_\infty$. The blue and red iso-surfaces correspond to positive and negative streamwise vorticity respectively.

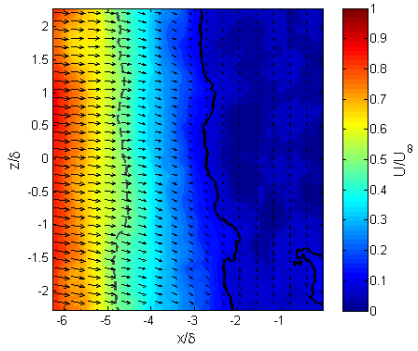

(a) Uncontrolled interaction

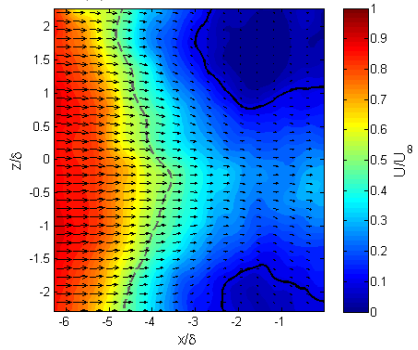

(b) Controlled interaction

Figure 3. Mean streamwise velocity contours U/U_∞ at y/δ =0.3. Black line encloses the $U<0.1\ U_\infty$ region and grey line indicates the M=1 isoline.

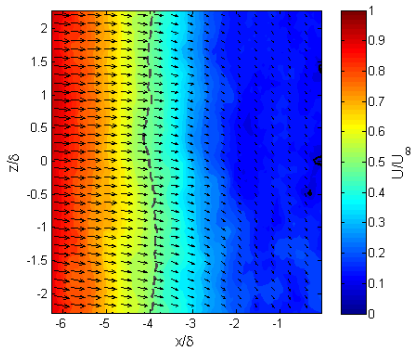

(a) Uncontrolled interaction

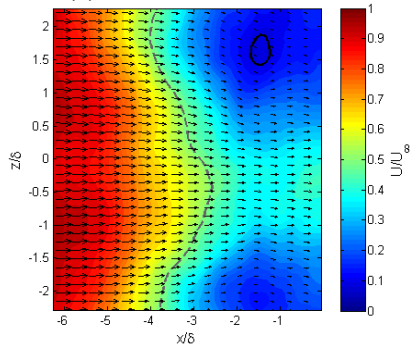

(a) Controlled interaction

Figure 4. Mean streamwise velocity contours U/U_∞ at y/δ =0.5. Black line encloses the $U<0.1\ U_\infty$ region and the grey line indicates the M=1 isoline.

Contours of the mean streamwise and wall-normal velocity are shown along a crossflow plane at the start of the measurement volume x/δ = -6.2 in Fig. 5. The micro-ramp wake that is approaching the interaction is a circular structure containing the counter-rotating vortices and is bound by a shear layer as shown in Fig. 5a. The primary counter-rotating vortices induce a mutual upwash attaining a maximum velocity of $V = 0.08U_\infty$ as can be seen in Fig. 5b. Further, it can be observed that the downwash regions on either side of the centreline extend over a larger area and attain approximately half the intensity of the upwash, $V= -0.04U_\infty$. Due to the mutual upwash, the vortices lift away from the wall while moving downstream. This can be observed in Fig. 6 which shows the flow field at the location x/δ = -2.5. Further downstream, the primary counter-rotating vortices pass through the expansion fan caused by the incident shock-wave reflection at the M=1 isoline. While passing through the expansion fan, the flow is turned towards the wall (see Fig 7.).

4. SEPARATION PROBABILITY

The separation behaviour of the interaction is further investigated by determining the separation probability of the interaction P_{sep} [4] at different wall-parallel planes. The separation probability P_{sep} is defined as the probability that a certain point in the measurement volume shows instantaneous flow reversal, $U < 0$, as defined by [4].

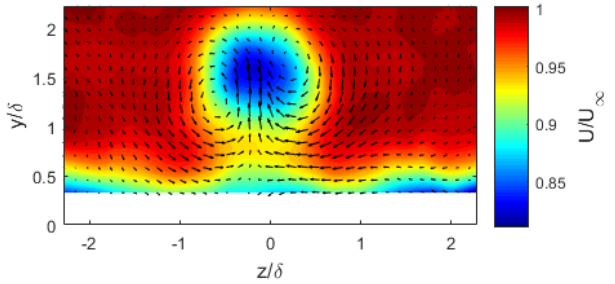

(a)

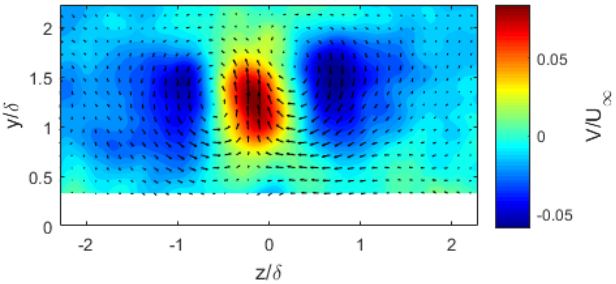

(b)

Figure 5. (a) Mean streamwise velocity contours U/U_∞ (b) Wall-normal velocity contours V/U_∞ at x/δ = -6.2 for the controlled interaction.

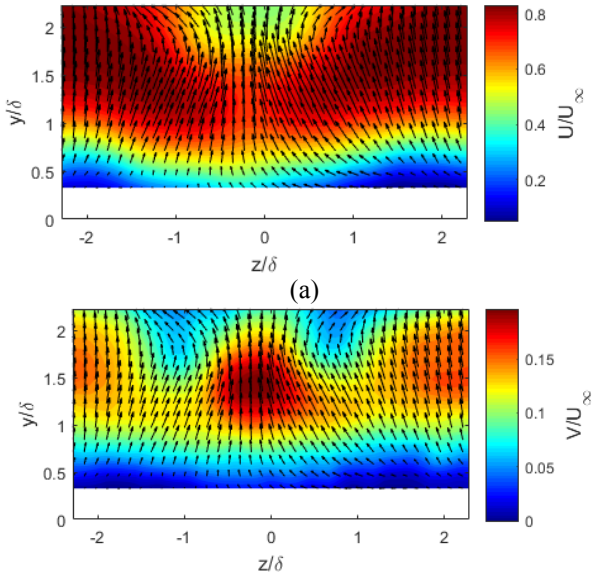

Figure 6. (a) Mean streamwise velocity contours U/U_∞ (b) Wall-normal velocity contours V/U_∞ at $x/\delta = -2.5$ for the controlled interaction.

Figs. 8 (a) and (b) show the separation probability P_{sep} for the uncontrolled and controlled interactions respectively at $y/\delta = 0.3$. The largest reductions in P_{sep} by using the micro-ramp control are observed close to the centreline, where the separation probability is reduced from 45% to 4%. At outboard locations ($|z/\delta| > 2$) the micro ramp is less effective and the separation probability has a similar value to that of the uncontrolled interaction.

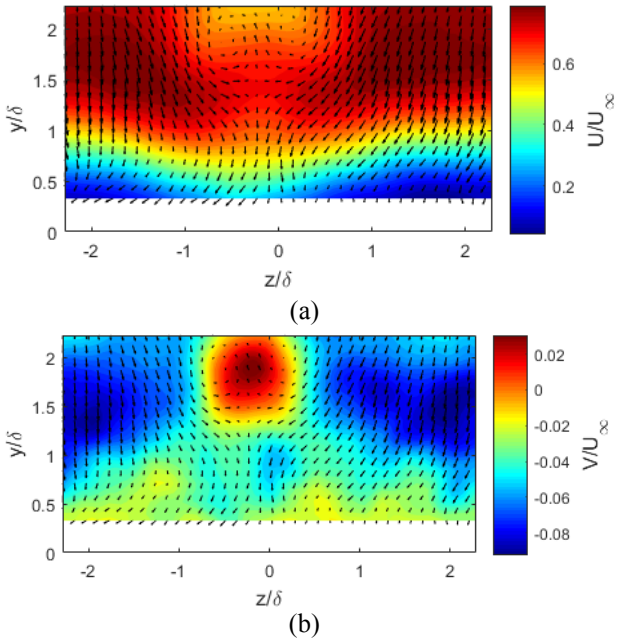

Figure 7. (a) Mean streamwise velocity contours U/U_∞ (b) Wall normal velocity contours V/U_∞ at $x/\delta = 0$ for the controlled interaction.

With increasing distance from the wall, the separation probability P_{sep} decreases. The separation probability for the uncontrolled and controlled interactions respectively at $y/\delta = 0.5$ is shown in Figs. 9 (a) and (b). At $y/\delta = 0.5$, the uncontrolled interaction shows a maximum P_{sep} = 35%. However, with micro-ramp control this maximum value is decreased to 31% (at $z/\delta = 1.5$) while there is no separation at the centreline. A similar decrease in P_{sep} is recorded at a wall normal location of $y/\delta = 0.75$ as can be seen in Figs. 10 (a) and (b). For $y/\delta = 0.75$, it is observed that the micro-ramp decreases the maximum P_{sep} from 21% to 14%. In this case also, there is no separation on the centreline.

Using the separation probability in the entire measurement volume, the total volume of separated flow V_{sep} , defined as the volume integration of P_{sep}, has been calculated. As result it is found that the micro-ramp control reduces the total volume of separated flow by 70% when compared to the uncontrolled interaction. This confirms that micro-ramps have a beneficial effect in reducing the total volume of separated flow.

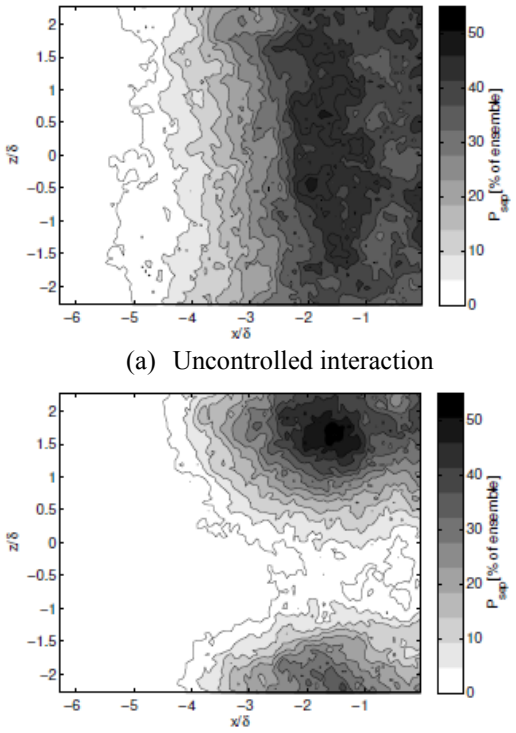

Figure 8. Separation Probability P_{sep} at $y/\delta = 0.3$. Flow direction is from left to right.

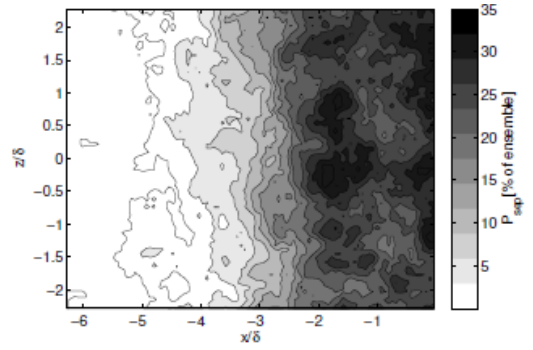

(a) Uncontrolled interaction

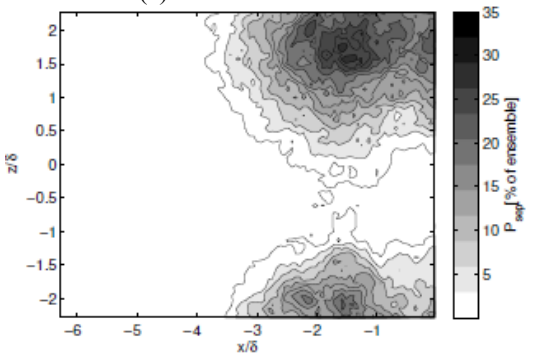

(b) Micro-ramp controlled interaction

Figure 9. Separation Probability P_{sep} at $y/\delta = 0.5$. Flow direction is from left to right.

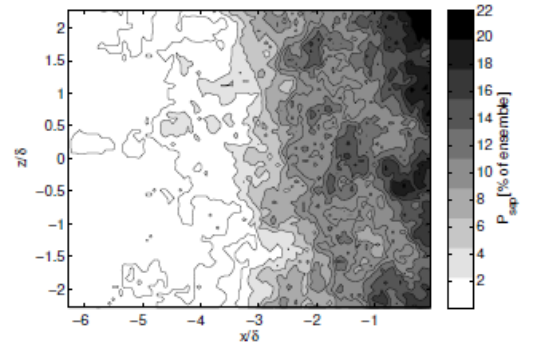

(a) Uncontrolled interaction

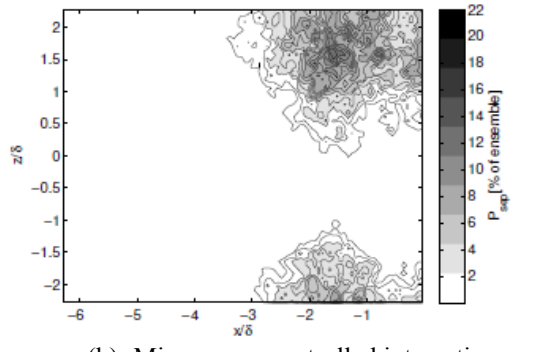

(b) Micro-ramp controlled interaction

Figure 10. Separation Probability P_{sep} at $y/\delta = 0.75$. Flow direction is from left to right.

5. CONCLUSION

A tomographic-PIV investigation was performed to visualize the 3D flow organization in an oblique shock wave-boundary layer interaction controlled by a single micro-ramp placed $17.3\delta_{99}$ upstream of the interaction. The mean streamwise and wall-normal velocity components were presented at various wall-parallel and crossflow slices, and the 3D modulation of the separation bubble was visualized. The probability of separation P_{sep} was also determined for the entire measurement volume. The largest reduction in separation probability P_{sep} occurs along the centreline of the micro-ramp. Further, it was found that a 70% reduction in shock-induced separation can be obtained by employing micro-ramp control when compared to an uncontrolled interaction. In addition to the results presented here on the interaction control by a single micro-ramp, it would be important to characterize the 3D flow fields for SWBLIs controlled by micro-ramp arrays in order to take into account mutual interactions, and the work for this is presently underway.

6. REFERENCES

[1] D. S. Dolling. Fifty years of shock-wave/boundary-layer interaction research: what next? *AIAA Journal*, 39(8), 1517–1531, 2001.

[2] J. Seddon and E. L. Goldsmith. *Intake aerodynamics*. 2nd ed, Blackwell Science, Boston, 1999.

[3] H. Babinsky, Y. Li, and C. W. Pitt Ford. Microramp control of supersonic oblique shock-wave/boundary-layer interactions. *AIAA Journal*, 47(3), 668–675, 2009.

[4] R. H. M. Giepman, F. F. J. Schrijer, and B. W. van Oudheusden. Flow control of an oblique shock wave reflection with micro-ramp vortex generators: Effects of location and size. *Physics of Fluids*, 26(6), 066101, 2014.

[5] P. L. Blinde, R. A. Humble, B. W. van Oudheusden, and F. Scarano. Effects of microramps on a shock wave/turbulent boundary layer interaction. *Shock Waves*, 19(6), 507–520, 2009.

[6] S. Lee, M. K. Goettke, E. Loth, J. Tinapple, and J. Benek. Microramps upstream of an oblique-shock/boundary-layer interaction. *AIAA Journal,* 48(1), 104–118, 2010.

[7] G. E. Elsinga, F. Scarano, B. Wieneke, and B. W. van Oudheusden. Tomographic particle image velocimetry. *Experiments in Fluids*, 41(6), 933–947, 2006.

[8] G. E. Elsinga, R. J. Adrian, B. W. van Oudheusden and F. Scarano. Three-dimensional vortex organization in a high-Reynolds-number supersonic turbulent boundary layer. *Journal of Fluid Mechanics*, *644*, 35-60, 2010.

[9] R. A. Humble, G. E. Elsinga, F. Scarano and B.W. van Oudheusden. Three-dimensional instantaneous structure of a shock wave/turbulent boundary layer interaction. *Journal of Fluid Mechanics*, *622*, 33-62, 2009.

[10] Z. Sun, F.F.J. Schrijer, F. Scarano and B.W. van Oudheusden. The three-dimensional flow organization past a micro-ramp in a supersonic boundary layer. *Physics of Fluids,* 24 055105, 2012

[11] B. H. Anderson, J. Tinapple, and L. Surber Optimal control of shock wave turbulent boundary layer interactions using micro-array actuation. *AIAA Journal*, 3197:2006, 2006.